Estimation and Suppression of Dispersion-Induced Phase Noise in W-band Direct-Detection OFDM Radio-Over-Fiber Systems

Chia-Chien Wei, Chun-Ting Lin, Hou-Tzu Huang, Wan-Ling Liang, and Sien Chi

***Abstract*—This study experimentally investigated the impact of dispersion-induced phase noise (DPN) on the transmission performance of a 100-GHz DD OFDM-RoF system. We sought to extend the transmission distance through the reduction of DPN using two digital phase noise suppression (PNS) schemes, based on the assumption that all subcarriers suffer from common DPN. The decision-aided PNS (DA-PNS) scheme treats the OFDM signal as feedback to aid in the calculation of DPN without incurring additional overhead. Pilot-aided PNS (PA-PNS) estimates the common DPN by inserting an additional optical pilot tone with guard band. Although both schemes are able to extend fiber transmission distance to beyond 150 km, the PA-PNS scheme tends to be outperformed by the DA-PNS scheme due to additional power required for the pilot tone. Nonetheless, in the DA-PNS scheme, the bandwidth of the estimated DPN must be truncated to avoid error propagation, which can result in the relatively faster increment in the transmission penalty. In contrast, the PA-PNS scheme maintains the variation in penalty to <1 dB, thereby achieving the performance that is insensitive to transmission distance.**

***Index Terms*—Direct detection, orthogonal frequency-division multiplexing (OFDM), radio-over-fiber system, W-band.**

I. Introduction

MILLIMETER waves, such as V-band (57–64 GHz) and W-band (75–110 GHz), have attracted considerable interest among researchers seeking to resolve increasing demands for bandwidth. These bands provide enormous un-licensed bandwidth of several GHz and the capacity to provide wireless transmission rates exceeding 10 Gbps [1]–[13]. Millimeter waves have also been considered as a possible solution to small-cell backhauling, which is likely to play an important role in bridging the capacity gap in the future [8]. Unlike the 60-GHz waves in the V-band, the 100-GHz waves in the W-band can be extended to outdoor communications thanks to less pronounced attenuation in air. Nonetheless, the 100-GHz transmission is still limited to light-of-sight. Radio-over-fiber (RoF) technology, combining the advantages of fiber and wireless techniques, has shown considerable promise in overcoming these limitations [9]–[13]. RoF technology is also viewed as an efficient means to simplify the implementation of remote units through infrastructural sharing. The need for spectral efficiency and multipath tolerance has led numerous researchers to combine orthogonal frequency-division multiplexing (OFDM) modulation with quadrature amplitude modulation (QAM) in order to increase capacity within wireless systems of limited bandwidth. [4]–[7], [11], [13].

Coherent detection (CO) [9]–[11] and direct detection (DD) [12], [13] are currently the primary methods used for the implementation of 100-GHz RoF systems. The use of an optical local oscillator (LO) in the CO scheme requires an additional laser and an optical hybrid coupler at remote nodes, which increases complexity and costs. In addition, the linewidth of both the transmitter laser and LO must be in the sub-MHz range in order to resist the influence of phase noise (PN), and frequency variations associated with lasers must be precisely controlled to generate mm-wave signals at the desired 100 GHz. As a result, the CO scheme is unsuitable for efforts to simplify remote units. In contrast, the DD scheme requires only a simple photodetector (PD) at a remote unit, making it far simpler and cost effective at the price of a more complicated transmitter. Generating the desired beating signal involves producing an RF tone and a modulated signal with 100-GHz frequency difference at the optical transmitter. Theoretically, if both of these were generated by modulating the same laser, the desired RF signal would be unaffected by laser PN following photo-detection. However, after fiber transmission, chromatic dispersion can produce walk-off in the time domain between the signal and the RF tone. This can result in degraded signal performance due to differential laser PN [14], [15], particularly when using an inexpensive commercial DFB laser with linewidth of several MHz. The fact is that dispersion-induced relative time delay is proportional to the difference in frequency between the RF tone and the signal. Thus, this issue is of greater consequence in W-band RoF systems than in lower frequency RoF systems and baseband optical OFDM systems. Several approaches have been developed to deal with phase noise suppression (PNS) through the estimation and elimination of PN in wireless and optical OFDM systems [16]–[24]. The key assumption in these approaches is that all OFDM subcarriers suffer the same PN, which is fallacious, considering the fact that fiber dispersion also de-correlates the PN of

Manuscript received January 15, 2014; revised April 18, 2014 and April 1, 2014; accepted March 5, 2014. Date of publication May 7, 2014; date of current version September 1, 2014. This work was supported in part by the National Science Council, Taiwan under Contract NSC 100–2221-E-110–089-MY3, NSC 101–2628-E-110–006-MY3, NSC 100–2628-E-019-MY3, and NSC 99–2221-E-009 -046-MY3.

C.-C. Wei is with the Department of Photonics, National Sun Yat-sen University, Kaohsiung 804, Taiwan (e-mail: ccwei@mail.nsysu.edu.tw).

C.-T. Lin, H.-T. Huang, and W.-L. Liang are with Institute of Photonic System, National Chiao Tung University, Hsinchu City 300, Taiwan (e-mail: jinting@mail.nctu.edu.tw; whang.kurt@gmail.com; liz-liang@hotmail.com).

S. Chi is with the Institute of Electro-Optical Engineering, and Institute of Photonic System, National Chiao Tung University, Hsinchu City 300, Taiwan (e-mail: schi@mail.nctu.edu.tw).

Color versions of one or more of the figures in this paper are available at http://ieeexplore.ieee.org.

Digital Object Identifier 10.1109/JLT.2014.2322601

subcarriers. In an RoF system, the OFDM bandwidth is relatively small compared to the RF frequency and as such this assumption may not be very far from the mark. Thus, the effectiveness of PNS schemes in a W-band RoF system warrants further investigation and experimental verification.

This study experimentally investigated the impact of dispersion-induced PN (DPN) on the transmission performance of a 100-GHz OFDM-RoF system. We employed two PNS approaches for the suppression of DPN caused by 1.5∼10.3-MHz-linewidth laser and 0∼150-km single-mode fiber transmission. By making hard decisions to obtain demodulated OFDM data, decision-aided PNS (DA-PNS) utilizes the deviation between the received and the demodulated data to estimate the DPN without incurring the additional overhead associated with optical power and electrical/optical components [17]–[20]. Pilot-aided PNS (PA-PNS) inserts an optical pilot tone to record phase noise as well as a guard band between the pilot tone and OFDM subcarriers to prevent the desired DPN information from being corrupted by OFDM subcarriers [21]–[24]. This study tested a 100-GHz OFDM-RoF signal with fixed QPSK format and 8.5-GHz bandwidth, which was insufficient to attain the FEC limit; i.e., a bit-error rate (BER) of 3.8×10^{-3}, with a laser linewidth of 10.3 MHz and distance of >100 km. Implementation of these schemes enabled the extension of the maximum fiber transmission distance (followed by 2-m air transmission) to beyond 150 km with sensitivity penalties of <∼2 dB. A comparison of the two schemes revealed that the DA-PNS scheme outperform the PA-PNS scheme due to the additional power required for the pilot tone. For the same reason, the signal with the PA-PNS scheme may underperform the signal without PNS, if the DPN is not crucial. To avoid the propagation of decision errors, the DA-PNS scheme requires that the bandwidth of the estimated DPN be truncated. This results in the relatively faster increment in the transmission penalty caused by residual DPN, while the PA-PNS scheme maintains this penalty variation to <1 dB. As a result, the OFDM signal with 1.5∼10.3-MHz linewidth in the PA-PNS scheme is insensitive to transmission distance within a range of 0∼150 km.

The remainder of the paper is organized as follows. Section II provides a theoretical discussion of PN caused by the interplay between laser PN and fiber dispersion. Section III introduces the two PNS schemes. Section IV presents the experimental setup of the 100-GHz DD OFDM-RoF system with and without an additional pilot tone. Section V outlines the experimental results. Section VI summarizes and concludes this paper.

II. Analysis of DPN

Without considering nonlinearity of optical modulators, an ideal optical DD OFDM-RoF signal is composed of an RF tone and *N* OFDM subcarriers, which are coherent due to their generation from the same laser. Intentionally setting the frequency difference between the RF tone and the OFDM signal as 100 GHz, the desired 100-GHz RF signal can be obtained without any laser-relevant PN after simple square-law photodetection. After wireless transmission and down-conversion of the RF signal, and the cyclic prefix (CP) removal and discrete Fourier transform (DFT) in the OFDM demodulation process, the received *q*th OFDM subcarrier can be represented as

$$Y_q = H_q X_q + W_q \tag{1}$$

where X_q, H_q and W_q are the transmitted QAM data, the channel response and the white noise of the *q*th subcarrier. Moreover, to simplify the dispersion effect in a DD OFDM system, each OFDM subcarrier is approximated a monochromatic wave with specific amplitude and phase according to the QAM data. Then, the dispersion effect can be simply viewed as creating different time delays among the RF tone and the subcarriers, as show in Fig. 1(a). Owing to the relative time delay, the beating result of photo-detection between the RF tone and a subcarrier will experience the differential laser PN, i.e. the DPN. As a result, the differential PN between the RF-tone and the *q*th subcarrier can be represented as $\varphi_q(t) = \theta(t + t_q) - \theta(t)$, where $\theta(t)$ and t_q are the laser PN and the dispersion-induced relative time delay between the RF-tone and the *q*th subcarrier, respectively. Because of the DPN, the *n*th received sampled point of the *q*th subcarrier needs to be multiplied by $\exp(j\phi_q(n))$ in the time domain, where $\phi_q(n) \equiv \varphi_q(n\Delta t)$ is the *n*th sampled DPN at the sampling rate of $1/\Delta t$ (set as the bandwidth of the OFDM signal). Therefore, the subcarrier after DFT will be circularly convolved with $\Phi_q(k)$ in the frequency domain, where $\Phi_q(k)$ is the *k*th discrete frequency component of $\exp(j\phi_q(n))$, i.e.

$$\Phi_q(k) = \frac{1}{N}\sum_{n=0}^{N-1} e^{j\phi_q(n)} e^{-j\frac{2\pi}{N}nk}. \tag{2}$$

Thus, the DPN experienced by the *q*th subcarrier will affect itself by $\Phi_q(0)$, which, assuming DPN is small, is generally approximated as

$$\Phi_q(0) = \frac{1}{N}\sum_{n=0}^{N-1} e^{j\phi_q(n)} \cong 1 + j\frac{1}{N}\sum_{n=0}^{N-1}\phi_q(n) \cong e^{j\bar{\phi}_q} \tag{3}$$

where $\bar{\phi}_q$ is the average of the sampled DPN. Equation (3) implies that the demodulated *q*th subcarrier will suffer phase error (PE), $\bar{\phi}_q$. Unlike [17], [18], [21], [22], however, the PE is not common among subcarriers due to their different time delays. Besides, the DPN also causes subcarrier expansion in the frequency domain to result in inter-carrier interference (ICI). Since the *m*th subcarrier will interfere the *q*th subcarrier through $\Phi_m(q-m)$, (1) would be modified as [14], [15]

$$Y_q \cong H_q X_q \exp(j\underbrace{\bar{\phi}_q}_{\mathrm{PE}}) + \underbrace{\sum_{m=0, m\neq q}^{N-1} H_m X_m \Phi_m(q-m)}_{\mathrm{ICI}} + W_q \ . \tag{4}$$

To evaluate PE and ICI, the variance is one of the most important parameters to be investigated. Since the laser PN $\theta(t)$ is generally modelled by the Wiener process [25], [26], ϕ_q is a stationary Gaussian process with the variance of $2\pi\beta t_q$, where β is the 3-dB laser linewidth. Using the autocorrelation function of ϕ_q: $R_{\phi_q}(\Delta n) = 2\pi\beta \cdot \max(0,\ t_q - |\Delta n|\Delta t)$, the variances

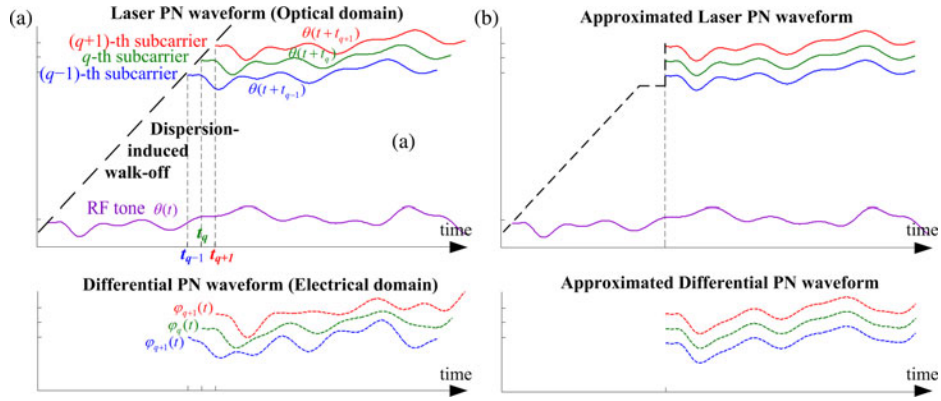

Fig. 1. Schematic plots of (a) dispersion-induced walk-off and the corresponding PN, and (b) the approximated case.

of $\bar{\phi}_q$ and $\Phi_q(k)$ can be derived as [15]

$$\sigma^2_{\mathrm{PE}}(q) = E\left[\bar{\phi}_q^2\right] = \frac{2\pi\beta}{N^2}\left[Nt_q + 2\sum_{\Delta n=1}^{\leq N-1 \atop \leq t_q/\Delta t}(N-\Delta n)\,(t_q - \Delta n\,\Delta t)\right] \tag{5}$$

$$E\left[|\Phi_q(k)|^2\right] = \frac{1}{N} + \frac{2}{N^2}\sum_{\Delta n=1}^{N-1}(N-\Delta n)\cos\left(\frac{2\pi}{N}\Delta n\,k\right)e^{-2\pi\beta\min(\Delta n\Delta t,\,t_q)} \tag{6}$$

where $E[\cdot]$ indicates the expectation value. Moreover, as the ICI power depends on both the characteristics of DPN and subcarrier data, the simplest case is that the subcarriers are of equal detected power, i.e. $E[H_q S_q H^*_{q'} S^*_{q'}] = P_D\,\delta_{q,q'}$, where $\delta_{q,q'}$ denotes the Kronecker delta. Then, the normalized power of ICI can be represented as [14], [15], [26]

$$\tilde{\sigma}^2_{\mathrm{ICI}}(q) = \frac{\sigma^2_{\mathrm{ICI}}(q)}{P_D} = \sum_{m=0,m\neq q}^{N-1} E\left[|\Phi_m(q-m)|^2\right]. \tag{7}$$

According to (5)–(7), the variances of PE and ICI are plotted in Fig. 2(a) and (b), respectively, in which the frequency difference between the RF tone and an 8.5-GHz OFDM signal of 362 subcarriers is 103 GHz. Since the variances would not be identical for each subcarrier, the maximum and the minimum values are plotted to exhibit the ranges. Both the variances of PE and ICI are about proportional to the laser linewidth, but the variance of PE increases with a higher slope after longer transmission in Fig. 2(a), in contrast to the roughly linear slope of ICI in Fig. 2(b). Actually, with additional assumptions of relatively small dispersion ($t_q \ll N\Delta t$) and relatively narrow bandwidth ($1/\Delta t \ll$100 GHz), the variances of (5) and (7) can be further approximated respectively as [15]

$$\sigma^2_{\mathrm{PE}}(q) \cong \frac{2\pi\beta t_q^2}{N\Delta t} \quad \text{and} \quad \tilde{\sigma}^2_{\mathrm{ICI}}(q) \cong 2\pi\beta t_q\,. \tag{8}$$

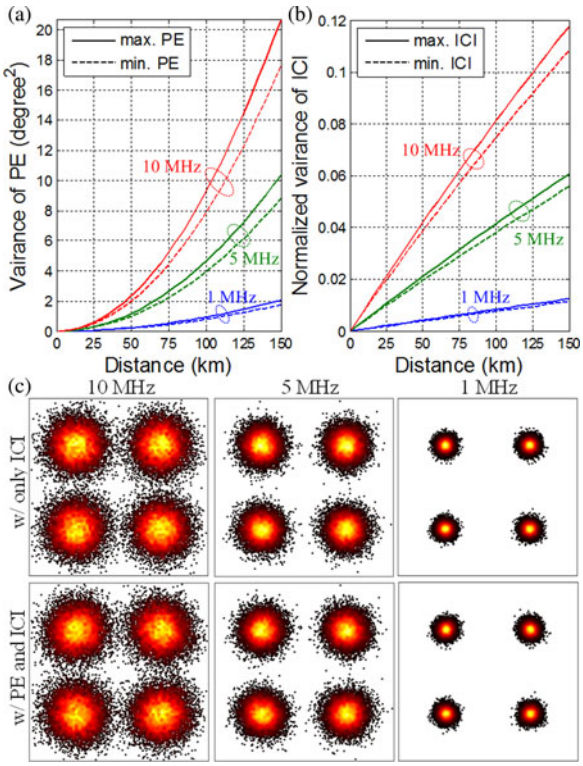

Fig. 2. Theoretical (a) PE and (b) ICI power after 0 ~ 150-km single-mode fiber, and (c) the Gaussian-approximated constellation diagrams after 150 km.

Assuming ICI and PE are Gaussian-distributed for simplicity and based on the theoretical variances in Fig. 2(a) and (b), some constellation diagrams with ICI only or with both PE and ICI are shown in Fig. 2(c) for comparison. These examples imply that ICI may dominate the transmission performance, even though PE increases faster. Moreover, as using a commercially available DFB laser of several MHz linewidth, Fig. 2 presents that the DPN could deteriorate the RoF signal after ~100 km, instead of hundreds to thousands of kilometers for optical baseband OFDM signals [14]. This is mainly because the relative time delay is proportional to the frequency difference between the RF tone

and the OFDM signal, and the frequency difference of 100 GHz in a W-band RoF system is much larger than that of ~10 GHz in a baseband OFDM system. Consequently, to improve the transmission performance of W-band DD OFDM-RoF systems, a PNS scheme would be necessary. Notably the assumption of Gaussian-distributed ICI may underestimate the influence of the DPN on the BER performance [14], [15]. However, further discussion on developing practical and precise BER estimation is out-of-scope of this paper. Another noteworthy feature of Fig. 2(a) and (b) is that, even though subcarriers suffer different DPN, the variance differences among subcarriers is relatively smaller than the variances.

III. Principle of Digital PNS Schemes

As mentioned that subcarriers would experience different dispersion-induced relative time delays, the DPN of each subcarrier would be different, such that the DPN estimation will be a very complicated task. Fortunately, the frequency differences among the subcarriers (i.e. the OFDM bandwidth, e.g. $\Delta f =$ 8.5 GHz in Fig. 2) are much smaller than that between the RF tone and the OFDM signal (i.e. the RF frequency, e.g. $f_{RF} =$ 103 GHz in Fig. 2) in a W-band RoF system. As a consequence, $\phi_q(n)$ and $\phi_{q\prime}(n)$ might be highly correlated. According to the properties of the Wiener process, the covariance of $\phi_q(n)$ and $\phi_{q\prime}(n)$ is $2\pi\beta \cdot \min(t_q,\ t_{q\prime})$, and the correlation coefficient is

$$\rho_\phi(q, q') = \frac{2\pi\beta \cdot \min(t_q,\ t_{q'})}{\sqrt{2\pi\beta t_q \times 2\pi\beta t_{q'}}} = \frac{\min(t_q,\ t_{q'})}{\sqrt{t_q \times t_{q'}}}\ . \tag{9}$$

As the relative time delay is proportional to the frequency difference, the minimum correlation coefficient is $\rho_\phi(0, N-1)$. Based on the nature of $\Delta f \ll f_{\mathrm{RF}}$ in a W-band system, the minimum correlation coefficient can be approximated as

$$\rho_\phi(0, N-1) = \frac{f_{RF} - \frac{\Delta f}{2}}{\sqrt{\left(f_{RF} - \frac{\Delta f}{2}\right)\left(f_{RF} + \frac{\Delta f}{2}\right)}} \cong 1 - \frac{\Delta f}{2 f_{RF}}\ . \tag{10}$$

Then, using the parameters in Fig. 2 as an example, the correlation coefficients of $\phi_q(n)$ and $\phi_{q\prime}(n)$ are always higher than ~0.96. Therefore, the DPN could be approximated to common one irrelevant to the frequencies of subcarriers [19], [20], [23], and

$$\phi_q(n) \cong \psi(n) \quad \text{and} \quad \Phi_q(k) \cong \Psi(k) \tag{11}$$

The simplification of (11) will be helpful in DPN estimation and suppression, and the corresponding simplified schematic plot of dispersion effect is exhibited in Fig. 1(b) to be compared with Fig. 1(a).

A. Concept of DA-PNS

Without any additional overhead and modification of an optical RoF signal, a DA-PNS scheme aims to estimate the DPN through identifying the relation between the transmitted and the received data. When the orthogonality among subcarriers will be destroyed by ICI, the subcarriers turn to be related to each other according to (4). To consider all the subcarriers simultaneously, (4) could be rewritten as a compact matrix form: $\mathbf{Y} = \hat{\mathbf{\Phi}}\mathbf{D} + \mathbf{W}$, where a hat is used to differentiate a matrix from a vector, and it is detailed in (12) shown at the bottom of the page. $D_q \equiv H_q X_q$ in (12) denotes the detected qth subcarrier without noise. Although the DPN matrix $\hat{\mathbf{\Phi}}$ consists of N^2 different entries, applying the approximated degeneracy in (11), the DPN matrix $\hat{\mathbf{\Phi}}$ could be simplified as

$$\tilde{\mathbf{\Psi}} = \begin{bmatrix} \Psi(0) & \Psi(N-1) & \Psi(N-2) & \cdots & \Psi(1) \\ \Psi(1) & \Psi(0) & \Psi(N-1) & \cdots & \Psi(2) \\ \Psi(2) & \Psi(1) & \Psi(0) & \cdots & \Psi(3) \\ \vdots & \vdots & \vdots & \ddots & \vdots \\ \Psi(N-1) & \Psi(N-2) & \Psi(N-3) & \cdots & \Psi(0) \end{bmatrix} \tag{13}$$

where the tilde denotes that a circulant matrix $\tilde{\mathbf{A}}$ is constructed by a vector $\mathbf{A}$. The circulant matrix $\tilde{\mathbf{\Psi}}$ in (13) is constructed by the vector of the DPN frequency components, $\mathbf{\Psi} = [\Psi(0),\ \Psi(1),\ \Psi(2),\ \ldots,\ \Psi(N-1)]^T$. Based on (13), the matrix production in (12) becomes $\tilde{\mathbf{\Psi}}\mathbf{D}$ and represents the matrix form of discrete circular convolution of $\mathbf{\Psi}$ and $\mathbf{D}$. Due to the commutativity of convolution, $\tilde{\mathbf{\Psi}}\mathbf{D}$ can be written as $\tilde{\mathbf{D}}\mathbf{\Psi}$, where $\tilde{\mathbf{D}}$ is a circulant matrix constructed by $\mathbf{D}$. At this point, assuming $\mathbf{D}$ can be known, the DPN $\mathbf{\Psi}$ can be estimated from the received subcarriers $\mathbf{Y}$ via the maximum likelihood estimation (MLE) of $\tilde{\mathbf{D}}^{-1}\mathbf{Y}$ [17], and the PNS may be achieved via $\tilde{\mathbf{\Psi}}^{-1}\mathbf{Y}$, where the superscript of -1 denotes the matrix inversion. In order to obtain the knowledge of $\mathbf{D}$, H_q and X_q can be estimated by training symbols and making hard decisions on $H_q^{-1}Y_q$, respectively. Denoting the decision result as $\mathbf{D}^{(0)}$, the estimated DPN is $\mathbf{\Psi}^{(0)} = (\tilde{\mathbf{D}}^{(0)})^{-1}\mathbf{Y}$.

Employing the estimated DPN to realize PNS, however, does not help better estimation of the transmitted data X_q, due to $(\tilde{\mathbf{\Psi}}^{(0)})^{-1}\mathbf{Y} = \mathbf{D}^{(0)}$. In other words, the decision errors in $\mathbf{D}^{(0)}$ will propagate to $\mathbf{\Psi}^{(0)}$ and back to $(\tilde{\mathbf{\Psi}}^{(0)})^{-1}\mathbf{Y}$. Therefore, the DA-PNS scheme requires the other assumption of limited DPN bandwidth such that the ICI bandwidth is truncated to reduce the effect of error propagation. The bandwidth truncation is realized by assuming only $2l+1$ nonzero low-frequency elements in $\mathbf{\Psi}$, or replacing $\mathbf{\Psi}$ by $\mathbf{\Psi}' = [\Psi(0),\ \ldots,\ \Psi(l),\ 0,\ \ldots, 0,\ \Psi(N-l),\ \ldots, \Psi(N-1)]^T$, where $2l+1 \le N$. In this way, (12) will

$$\begin{bmatrix} Y_0 \\ Y_1 \\ Y_2 \\ \vdots \\ Y_{N-1} \end{bmatrix} = \begin{bmatrix} \Phi_0(0) & \Phi_1(N-1) & \Phi_2(N-2) & \cdots & \Phi_{N-1}(1) \\ \Phi_0(1) & \Phi_1(0) & \Phi_2(N-1) & \cdots & \Phi_{N-1}(2) \\ \Phi_0(2) & \Phi_1(1) & \Phi_2(0) & \cdots & \Phi_{N-1}(3) \\ \vdots & \vdots & \vdots & \ddots & \vdots \\ \Phi_0(N-1) & \Phi_1(N-2) & \Phi_2(N-3) & \cdots & \Phi_{N-1}(0) \end{bmatrix} \times \begin{bmatrix} D_0 \\ D_1 \\ D_2 \\ \vdots \\ D_{N-1} \end{bmatrix} + \begin{bmatrix} W_0 \\ W_1 \\ W_2 \\ \vdots \\ W_{N-1} \end{bmatrix}. \tag{12}$$

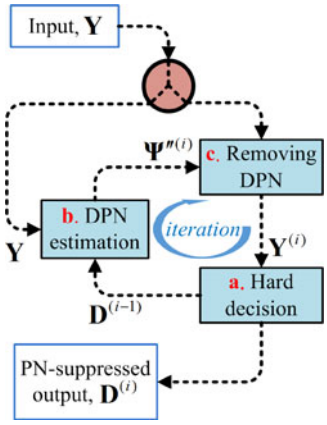

Fig. 3. The flow chart of the DA-PNS scheme.

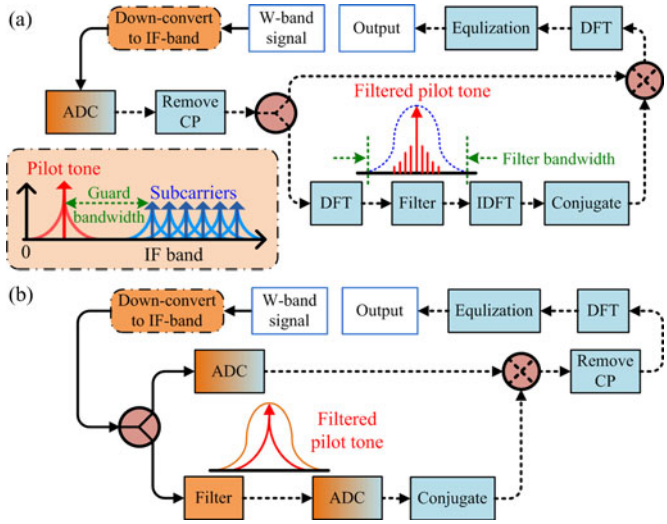

Fig. 4. The flow chart of the PA-PNS scheme using (a) digital filtering or (b) analog filtering.

be rewritten as

$$\mathbf{Y} = \tilde{\boldsymbol{\Psi}}'\mathbf{D} + \mathbf{W}' = \tilde{\mathbf{D}}\boldsymbol{\Psi}' + \mathbf{W}' = \hat{\mathbf{D}}''\boldsymbol{\Psi}'' + \mathbf{W}' \tag{14}$$

where $\mathbf{W}' = (\tilde{\boldsymbol{\Psi}} - \tilde{\boldsymbol{\Psi}}')\mathbf{D} + \mathbf{W}$ is the summation of the residual ICI and the noise. In the last equality of (14), the zeros in $\boldsymbol{\Psi}'$ are removed to obtain $\boldsymbol{\Psi}'' = [\Psi(0), \ldots, \Psi(l), \Psi(N-l), \ldots, \Psi(N-1)]^T$ with the vector length of $2l+1$, and $\hat{\mathbf{D}}''$ is an $N \times (2l+1)$ matrix obtained by removing the $(l+2)$-th to $(N-l)$-th columns of $\tilde{\mathbf{D}}$, which correspond to the zeros in $\boldsymbol{\Psi}'$. As a result, after making hard decision to obtain $\mathbf{D}^{(0)}$ and $\hat{\mathbf{D}}^{(0)}$, $\boldsymbol{\Psi}''^{(1)}$ can be estimated by the MLE of $\boldsymbol{\Psi}''^{(1)} = (\hat{\mathbf{D}}''^{(0)})^{+}\mathbf{Y}$, where the superscript $+$ denotes the pseudoinverse. Accordingly, the "common" PE is estimated as the phase of the first element of $\boldsymbol{\Psi}''^{(1)}$ or $\angle\Psi^{(1)}(0)$, and the ICI is $(\tilde{\boldsymbol{\Psi}}'^{(1)} - \Psi^{(1)}(0)\cdot\hat{\mathbf{I}})\,\mathbf{D}^{(0)}$, where $\hat{\mathbf{I}}$ is an $N \times N$ identity matrix. Then, the PNS is realized via reversing the process of DPN disturbance shown in (4)

$$\mathbf{Y}^{(1)} = (\Psi^{(1)}(0))^{-1}[\mathbf{Y} - (\tilde{\boldsymbol{\Psi}}'^{(1)} - \Psi^{(1)}(0)\cdot\hat{\mathbf{I}})\,\mathbf{D}^{(0)}] \tag{15}$$

which is expected to perform better than the original received signal. Furthermore, an iterative process could be applied by using the new hard-decision result of $\mathbf{D}^{(i)}$ obtained from $\mathbf{Y}^{(i)}$ to replace the previous $\mathbf{D}^{(i-1)}$ in the algorithm, where $\mathbf{Y}^{(0)} \equiv \mathbf{Y}$, and the process may improve the accuracy of DPN estimation and suppression. The iterative algorithm of the DA-PNS is summarized in Fig. 3, and it contains following three iterative steps:

1) making hard decisions on the received signal to "guess" the ideal detected signal is $\mathbf{D}^{(i-1)}$;
2) estimating the DPN as $\boldsymbol{\Psi}''^{(i)}$ from the received signal and the guessed detected signal;
3) removing the DPN from the received signal by the estimated DPN to get a DPN-suppressed signal, $\mathbf{Y}^{(i)}$.

B. Concept of PA-PNS

With the same assumption of (11) illustrated in Fig. 1(b), all the subcarriers would experience the same DPN, even if some of them are used as pilot tones, of which the transmitted amplitudes and phases are known at the receiver. Therefore, taking the average of relative phase shifts of the received pilot tones with respect to the transmitted ones, the "common" PE could be estimated [21], where the average is required due to the presence of ICI and noise. As shown in Fig. 2, however, PE is not a major issue in a W-band DD RoF system. Hence, to fully estimate the DPN via a pilot-aided method, one pilot tone with sufficient guard band is required [21], [22]. When the delta-function-like spectrum of the pilot tone is broadened by the DPN, the requirement of only one pilot tone with sufficient guard band is because multiple neighboring tones, no matter known pilot tones or unknown OFDM subcarriers, will interfere the DPN carried by the pilot tone. Then, the DPN can be simply estimated by applying filter to the pilot tone. Ideally, the filtered pilot tone would be $\exp(j\varphi_p(t))$, where the DPN of the pilot tone is assumed to be identical to that of all the subcarriers, $\varphi_p(t) \cong \varphi_q(t)$. Besides, since only one pilot tone can be employed, the pilot tone of relative strong power is necessary to increase the pilot-to-noise ratio (PNR) and the accuracy of the DPN estimation. Denoting the PNR as γ_p, it has been shown that, in an additive white Gaussian noise (AWGN) channel, the variance of extra PN of the pilot tone caused by AWGN can be approximated as

$$\sigma^2_{PN,p} \cong \frac{1}{2\gamma_p}\,. \tag{16}$$

Therefore, if the filter bandwidth is increased to accommodate more frequency components of the DPN, more noise is also filtered to reduce the PNR and to increase undesired extra PN. This implies there would be a trade-off between these two effects in selecting the filter bandwidth. Fig. 4 shows the schematic plot of the PA-PNS scheme. The PNS is carried out by multiplying the conjugated version of the filtered pilot tone to the received OFDM signal in the time domain, i.e. the DPN subtraction by the estimated one, $\varphi_q(t) - \varphi_p(t)$. To realize filtering the pilot tone, there are two possible ways shown in Fig. 4(a) and (b). In Fig. 4(a), filtering is accomplished in digital domain. After removing the CP and employing DFT, the demodulated signal,

including the pilot tone, is multiplied to the discrete spectrum of a designed filter to preserve only the desired DPN carried by the pilot tone. Since the PNS is carried out in the time domain, inverse DFT (IDFT) is needed to convert the filtered DPN spectrum. On the other hand, as shown Fig. 4(b), filtering could be realized in analog domain through a suitable electrical filter, and its benefit is to avoid additional computational complexity caused by DFT and IDFT in Fig. 4(a). Nevertheless, the second approach requires an extra analog-to-digital converter (ADC) to process the filtered pilot tone, and this would be more undesired than additional DFT and IDFT. Consequently, the first approach is adopted in this paper.

C. Comparison of Computational Complexity Between PNS schemes

Most of the additional computational cost in the PA-PNS scheme comes from the digital filtering of the pilot tone, in which DFT and IDFT require $O(N \times \log_2 N)$ operations. DPN estimation in the DA-PNS scheme requires a matrix pseudoinverse, which dominates the computational complexity of the algorithm. This requires $O(N \times (2l+1)^2)$ floating-point operations, allowing for a further reduction in complexity using advanced algorithms. Since l is generally small (compared with N) [19], the truncation of DPN bandwidth in the DA-PNS scheme incidentally reduces computational complexity; however, the overall complexity is still higher than that of PA-PNS even without considering the multiple iterations, because $(2l+1)^2$ is generally larger than $\log_2 N$.

IV. Experimental Setup

The experimental setup of the W-band DD OFDM-RoF transmission system is presented in Fig. 5. Two single-drive Mach-Zehnder modulators (SD-MZMs) (Sumitomo, 40 GHz intensity modulator) were cascaded to generate the desired RoF signal. The optical light source was a commercially available DFB laser with variable linewidth, which was controlled by intentionally adjusting the laser output power. Using the delayed self-heterodyne technique [27], the linewidth was measured as 1.5, 5.5, or 10.3 MHz, when the laser output power was set to 13, 6, or 3 dBm, respectively. Both of the SD-MZMs were biased at the null-point to realize carrier-suppressed double sideband modulation. The transmitted OFDM signal was coded as QPSK, comprising 362 subcarriers with a DFT size of 512 and CP set to 1/16. The OFDM signal is complex; therefore, the baseband I-signal and Q-signal were generated in two independent channels (bandwidth of 4.25-GHz each), using an arbitrary waveform generator (AWG) (Agilent, M8190A) at a sampling rate of 12 GSample/s. Following up-conversion via an electrical I/Q mixer (Hittite Microwave, HMC-C046), an electrical RF OFDM signal of 8.5-GHz bandwidth was generated at 21.5 GHz. The OFDM signal was then combined with a 38.5-GHz electrical sinusoidal wave corresponding to the RF tone, whereupon the combined signal was used to modulate the first SD-MZM. Generating the required pilot tone in the PA-PNS scheme required that an additional electrical sinusoidal wave be combined with the driving signal of the first SD-MZM, and that its frequency be controlled to a range of 16.8 to 13.5 GHz, resulting in a guard band of 0.45 $\sim$ 3.75 GHz. It should be noted that the pilot tone was not inserted into the middle of the OFDM band as in [21]–[23], because the AWG or a general digital-to-analog converter has limited electrical bandwidth and is better able to generate subcarriers with a higher electrical signal-to-noise ratio (SNR) at lower frequencies. Thus, inserting a pilot tone outside the OFDM band generates an OFDM driving signal with similar electrical SNR in all cases with and without the PNS schemes, enabling a fair comparison of results. The spectra of the driving signal and corresponding optical signal are presented in insets (A) and (a) of Fig. 5, respectively. The second SD-MZM was modulated by the 21.5-GHz sinusoidal wave, enabling it to suppress the input optical signal and copy the original signal to the 21.5-GHz higher frequency as well as the 21.5-GHz lower frequency. The resulting optical spectrum is illustrated in inset (b) of Fig. 5, showing four duplicates of the RF tone and OFDM signal. Two duplicates of the OFDM signal overlap at the frequency of the laser, and the greatest difference in frequency between the RF tone and the OFDM signal is the desired 103 GHz. To maintain only the required RF tone and OFDM signal, all unnecessary carriers and signals are filtered out using an optical interleaver. The optical spectrum of the W-band DD OFDM-RoF signal is plotted in inset (c) of Fig. 5. To compensate the loss of SD-MZMs, an EDFA was inserted after each SD-MZM, and the EDFAs were included even at optical back-to-back (OBtB, only 2-m wireless transmission). After 0 $\sim$ 150-km single-mode fiber transmission, the optical signal was detected using a high-speed PD (u2t, XPDV4120R) with 3-dB bandwidth of 100 GHz to generate the desired electrical W-band RF signal. For 150-km transmission, two EDFAs were inserted after 50-km and 125-km transmission to compensate the fiber loss, and an optical bandpass filter with 100-GHz bandwidth was employed to reduce ASE noise. To focus on the issue of dispersion, optical attenuators were applied to fix the input power of the EDFAs for the transmission of $<$150 km such that all transmission cases suffered the same level of ASE noise, and all fiber launch powers were set 0 $\sim$ 4 dBm to prevent fiber nonlinearities. A pair of rectangular waveguide-based standard gain horn antennas with 24-dBi gain was employed to realize 2-m wireless transmission. Before and after wireless transmission, a customized low-noise amplifier was inserted, of which the gain, the voltage standing wave ratio and the passband are 24 dB, 1.2:1, and 75–100 GHz, respectively. Then, the received W-band signal was sent into an electrical bandpass filter of 14-GHz bandwidth centered at 100 GHz, before the signal was mixed with a 94.5-GHz electrical sinusoidal wave, the frequency of which is tripled using a frequency multiplier. Thus, the received signal was down-converted to 8.5 GHz, as shown in inset (B), and captured via a real-time scope (Tektronix, DSOX91604A) with 80-GSample/s sampling rate. Finally, an off-line digital signal processing was applied to demodulate the signal. Without inserting the pilot tone, no PNS scheme or the DA-PNS scheme was included in the off-line process. When the pilot tone was inserted, the off-line process included the PA-PNS scheme. Following the demodulation process, the SNR and BER were estimated. The BER was calculated by counting the number of errors, and

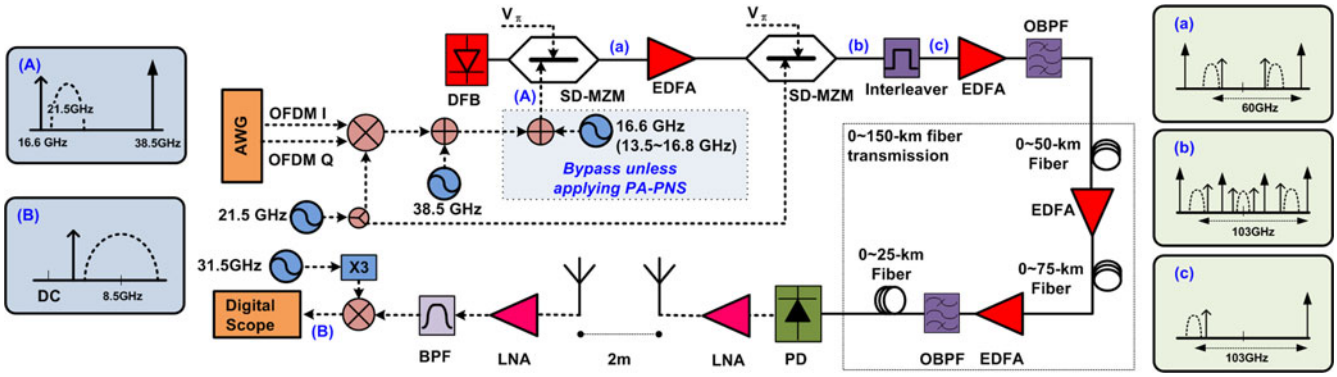

Fig. 5. Experimental setup.

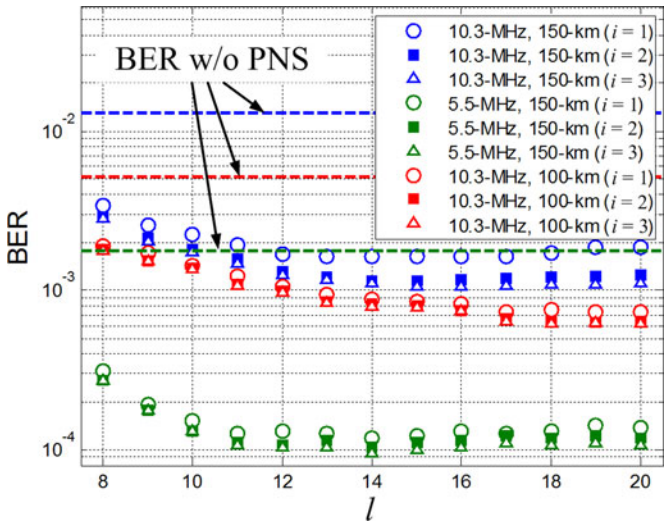

Fig. 6. BER with the DA-PNS scheme as a function of l.

more than 7×10^5 bits were transmitted for reliable BER measuring at the range of interest.

V. Experimental Results and Discussion

A. Optimization of DA-PNS

The DA-PNS scheme includes two major parameters (DPN bandwidth of $2l+1$ and the iterative number), which are related to the performance of PNS and the complexity of the algorithm. As shown in Fig. 6, investigating the performance dependency requires that BER be measured as a function of l with the received power of -6 dBm after 150-km fiber transmission and the DA-PNS. In Fig. 6, the optimized l is approximately 14∼18. The main reason for DPN bandwidth truncation is the avoidance of error propagation, such that the real DPN bandwidth could be much greater than $2l+1$. Thus, if l were lower than the optimized value, most of the desired DPN detail would be lost. Although the accuracy of DPN estimation could be improved by increasing l, the application of l exceeding the optimized value would lead to a reduction in BER resulting from error propagation from $\mathbf{D}^{(i-1)}$ to $\mathbf{D}^{(i)}$. It should be noted that, to achieve the best results, the optimized values of l would vary with transmission distance and laser linewidth, even with differences in iteration time. However, l can be optimized in advance using training symbols. As a result, l was optimized each time that the proposed algorithm was applied throughout the experiment, resulting in values falling between 10 and 20. In addition, the third iteration ($i=3$) provided little improvement, as show in Fig. 6; therefore, we can surmise that 3 iterations may be sufficient to achieve the usable result. When taking reasonable computational complexity into account as well, this study set the number of iterations to 3.

B. Optimization of PA-PNS

Compared with a simple raised-cosine filter, an adaptive Wiener filter has been demonstrated to provide only slightly superior performance [23]. In addition, an adaptive Wiener filter requires additional calculation and feedback, which increases complexity; therefore, this paper adopted a raised-cosine filter. This implies that, in the PA-PNS scheme, four parameters must be determined: the pilot-to-signal power ratio (PSPR), the bandwidth of the guard band, and the bandwidth and the roll-off factor of the raise-cosine filter. Optimizing the performance of the PA-PNS with regard to the four parameters is a difficult task. Following a series of trials, the PSPR, guard bandwidth as well as the bandwidth and roll-off factor of the filter were roughly determined as 1.8 dB, 0.65 GHz, 1.3 GHz, and 0.5, respectively. The guard bandwidth of 0.65 GHz indicates that the added sinusoidal wave is at a frequency of 16.6 $(=21.5-4.25-0.65)$ GHz. In Figs. 7–9, one or two of these parameters are changed while the others remain fixed to investigate the dependency of SNR on each parameter, with the laser linewidth, the received optical power, and fiber distance set to 10.3 MHz, -6 dBm, and 150 km, respectively. Fig. 7 presents the SNR of the OFDM signal as a function of the PSPR with an optimized value of ∼2 dB. Increasing the power of the added pilot tone produced two effects: 1) a reduction in the OFDM signal power resulting in a degradation in the SNR prior to the application of PA-PNS and 2) an increase in PNR resulting in improved DPN estimation. Thus, for a PSPR below ∼2 dB, the SNR decreased with an increase in PSPR, because the PNR is low, such that DPN information from the pilot tone is disturbed by noise. If the PSPR is higher

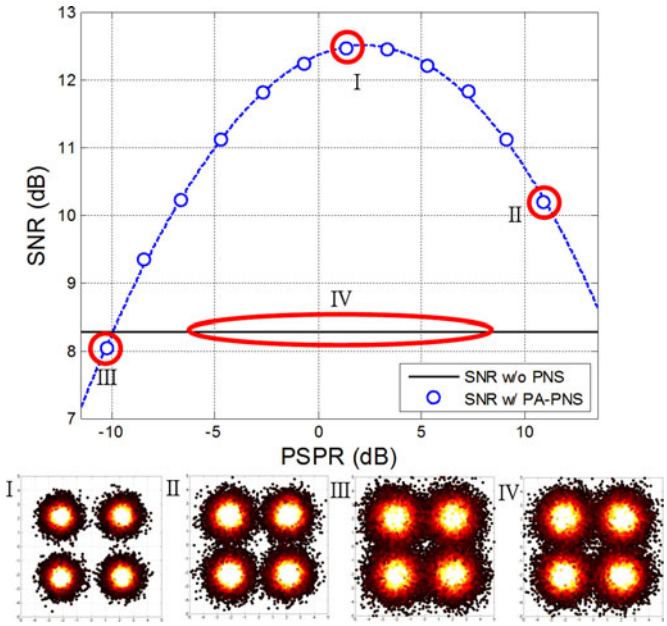

Fig. 7. SNR with the PA-PNS scheme as a function of PSPR.

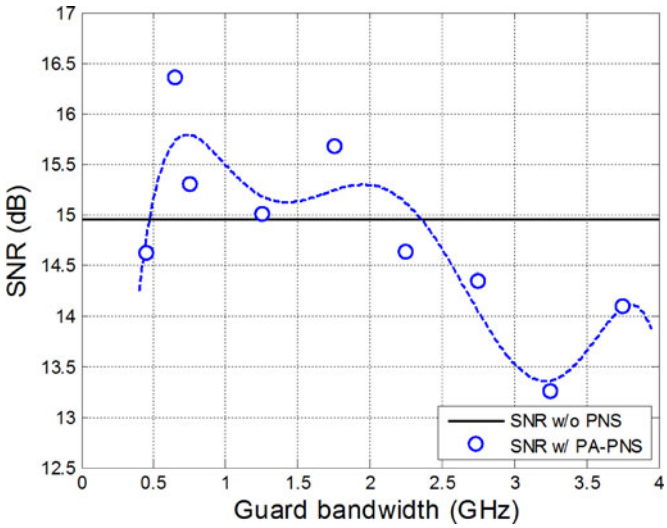

Fig. 8. SNR with the PA-PNS scheme as a function of guard bandwidth.

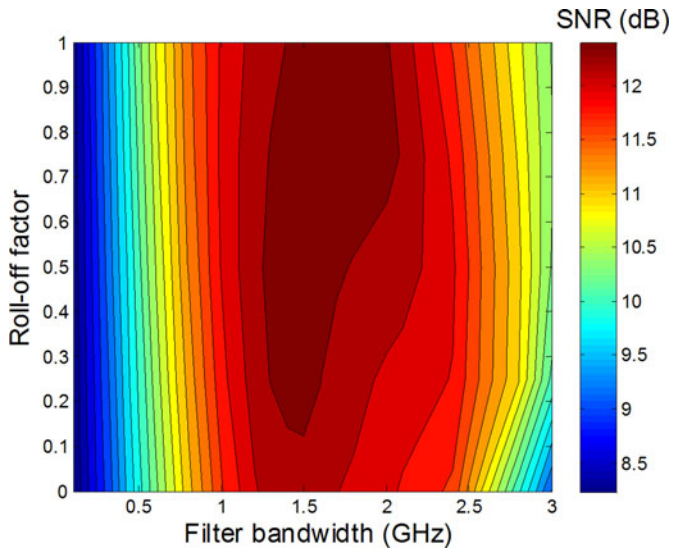

Fig. 9. SNR with the PA-PNS scheme as a function of the bandwidth and the roll-off factor of the filter.

than ~2 dB, the degraded SNR prior to PA-PNS dominates the SNR after PA-PNS. The constellations of the extreme cases are presented in Fig. 7. In Fig. 8, the SNR is measured as a function of guard bandwidth, and the filter bandwidth is set at a value of twice the guard bandwidth in order to prevent interference caused by the subcarriers. In principle, as the frequency components of the DPN fall to the level of noise, they are no longer required and should therefore be rejected by the filter. The optimized value of guard bandwidth in Fig. 8 is around 0.65 GHz. However, when the bandwidth deviates from its optimal value, the SNR does not decrease monotonically because the power spectrum of the DPN does not monotonically decrease with an increase in frequency. Fig. 9 exhibits the SNR as a contour plot with various bandwidths and roll-off factors of the filter, in which the bandwidth is optimized roughly just for filtering the OFDM signal. The results are less sensitive to the roll-off factor, as the roll-off factor of >0.1. When it is smaller than 0.1, however, the sharp edge of the band of the filter does not match the slow-varying DPN spectrum, resulting in degraded SNR values.

C. Performance Comparison Between PNS Schemes

Fig. 10 presents the BER curves after 150-km fiber transmission with DA- or PA-PNS and without PNS, and Fig. 10(a)–(c) exhibits cases with linewidths of 10.3, 5.5 and 1.5 MHz, respectively. When the laser linewidth was 10.3 MHz, the signal cannot achieve the FEC limit without the PNS schemes, and the BER is improved to below 3.8×10^{-3} using both of the PNS schemes. When the laser linewidth was 5.5 or 1.5 MHz, the signal without the PNS schemes achieved the FEC limit; however, both of the PNS schemes were able to lower the BER to improve sensitivity at the FEC limit. Fig. 10 presents the BER curves for OBtB. There is no DPN at OBtB; therefore, PNS is not necessary and the optimized l of the DA-PNS scheme is 0, such that the BER does not change after the DA-PNS. In the PA-PNS scheme, the signal at OBtB suffered approximately 1-dB sensitivity penalty due to the useless PA-PNS. With the application of the PNS process at OBtB, as illustrated in Fig. 4, the filtered pilot tone actually carries only undesired random noise. Consequently, the loss of sensitivity with the PA-PNS is due to the portion of the received power occupied by the pilot tone as well as additional distortion caused by the multiplication of the noisy pilot tone. In fact, the reduction in the signal power resulting from the addition of the pilot tone is the fundamental disadvantage of the PA-PNS scheme, resulting in lower signal SNR prior to the application of PNS. Thus, for the PA-PNS to achieve a performance improvement, the contribution from the PNS must exceed the loss in SNR. In contrast, the DA-PNS

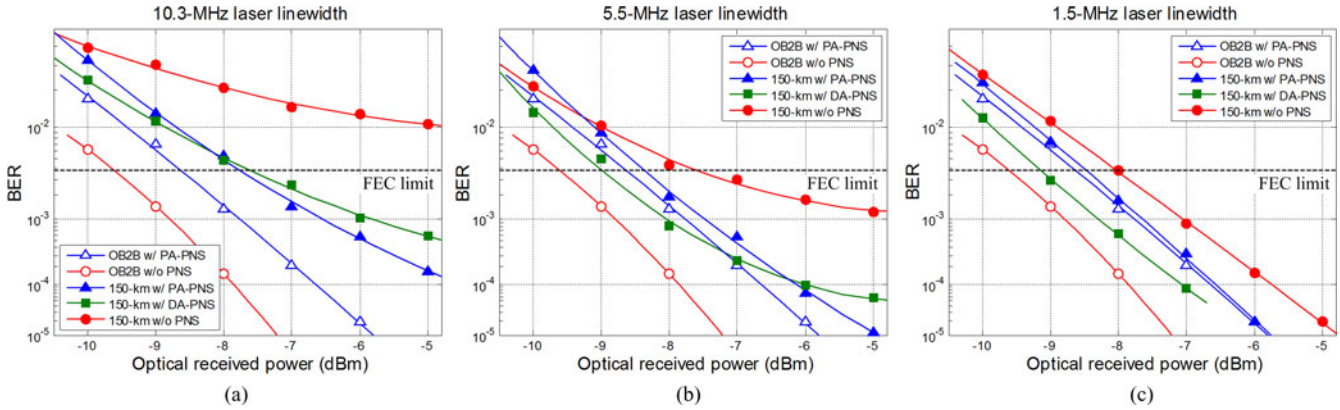

Fig. 10. BER curves with and without the PNS schemes after 150-km fiber transmission, and the laser linewidth is (a) 10.3 MHz, (b) 5.5 MHz, and (c) 1.5 MHz.

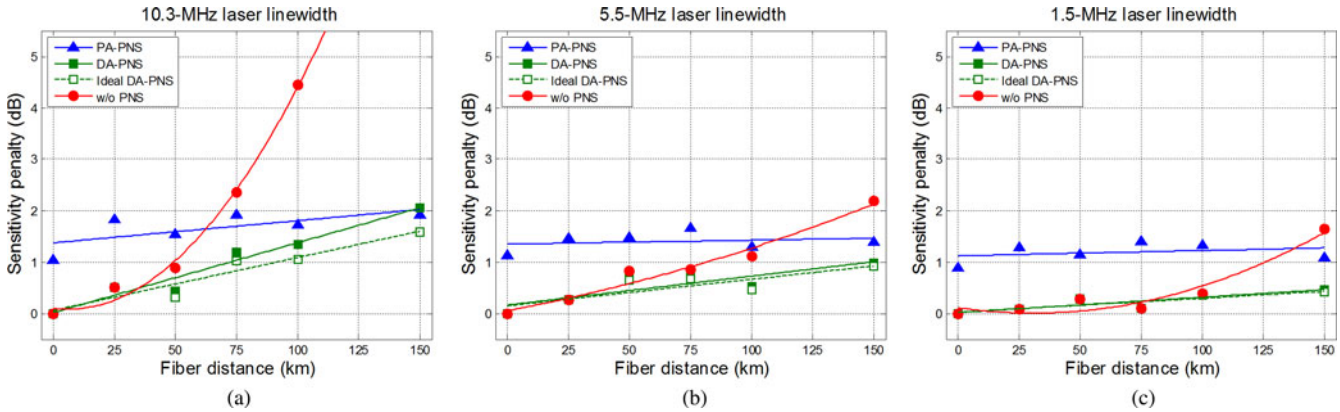

Fig. 11. The measured sensitivities as functions of fiber distance with laser linewidth of (a) 10.3 MHz, (b) 5.5 MHz, and (c) 1.5 MHz.

scheme requires no additional overhead; therefore, when DPN is relative less, such as in cases with linewidths of 1.5 and 5.5 MHz in Fig. 10(b) and (c), the DA-PNS scheme is able to decrease the BER more effectively than the PA-PNS scheme. Nonetheless, in cases in which the DPN is more serious [e.g. the case with linewidth of 10.3-MHz in Fig. 10(a)], the PA-PNS scheme may be able to outperform the other scheme, because the DPN bandwidth must be balanced against decision error propagation in the DA-PNS scheme. Notably the common assumption of the two PNS schemes is to neglect the difference of DPN among subcarriers, and this implies the perfect PNS is not possible.

Fig. 11 presents the relative sensitivity penalties associated with reaching the FEC limit as a function of fiber distance, with and without the PNS schemes. Fig. 11(a)–(c) presents cases with linewidths of 10.3, 5.5, and 1.5 MHz, respectively. In addition to the DA-PNS, an ideal DA-PNS employs the DA-PNS scheme with a perfect knowledge of $\mathbf{D}$, while l is kept identical to that adopted in the practical DA-PNS scheme. Thus, the difference between the practical DA-PNS and the ideal DA-PNS can be traced to whether or not decision error propagation exists. The limited difference implies that decision errors do not greatly affect the DA-PNS scheme at the important BER of 3.8×10^{-3}. As a result of DPN, transmission performance without PNS can be degraded over longer fiber distances and/or with wider laser linewidth. With a linewidth of 10.3 MHz, the transmission distance is limited to $\leq$100 km. Using the DA-PNS scheme, improvements can be observed after 100-, 50-, and $<$50-km with 1.5-, 5.5-, and 10.3-MHz linewidths, respectively. If the fiber distance is shorter than the above values, the relatively small contribution of the DPN to total noise at the FEC limit means that DA-PNS is not necessary. However, the fact that the truncation of DPN bandwidth is unavoidable, PNS cannot be perfect, such that even with the ideal DA-PNS scheme, the sensitivities are still slowly degraded by an increase in distance. As for the PA-PNS scheme, when the DPN is relatively small at shorter distances and/or with narrower linewidths, the major effect of inserting the pilot tone is a reduction in signal power and drop in SNR, with a corresponding maximum penalty of approximately 1 dB. Once the DPN becomes crucial, such as at distances of $\geq$75, $>$100 and $\geq$150 km in Fig. 11(a)–(c), respectively, the application of the PA-PNS scheme can improve sensitivity. Furthermore, both schemes can extend the transmission distance to beyond 150 km, even when a laser with a linewidth of 10.3-MHz is adopted. In contrast to the situation presented in Fig. 11, the transmission penalties (defined as the sensitivities related to themselves at OBtB), are plotted as a function of linewidth in Fig. 12. The results using various schemes are presented in Fig. 12(a)–(c). In Fig. 12(a), the transmission

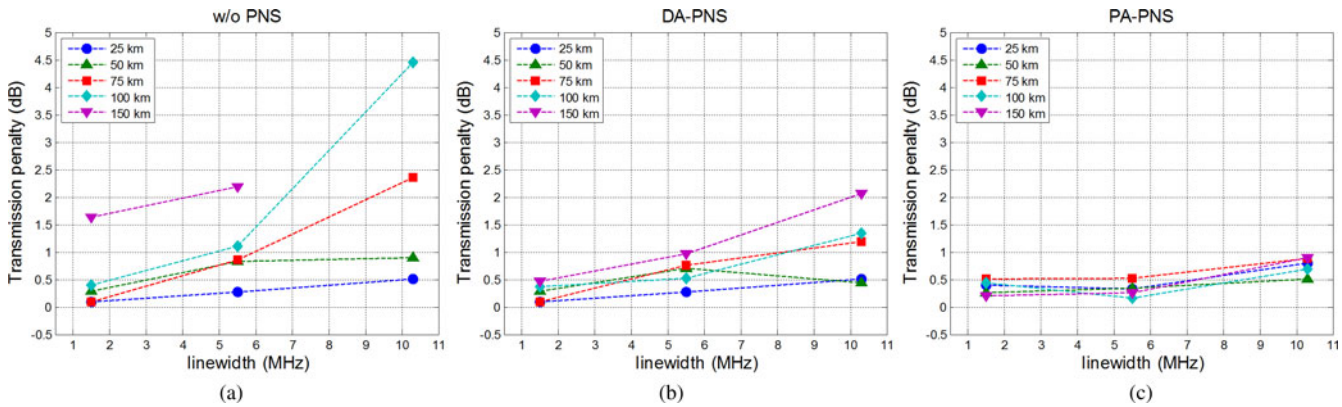

Fig. 12. The transmission sensitivities as functions of laser linewidth (a) without PNS, (b) with the DA-PNS scheme, and (c) with the PA-PNS scheme.

performance is deteriorated more by DPN with an increase in fiber distance and/or laser linewidth. In Fig. 12(b), the sensitivities are improved by the DA-PNS scheme; however, longer distances and/or wider linewidths still degrade performance. As shown in Fig. 12(c), employing the PA-PNS scheme resulted in all transmission penalties falling within the range of approximately 0.2 $\sim$ 0.9 dB. This small variation implies that the PA-PNS scheme is able to clamp the transmission performance, such that the variation in sensitivity is less than $\sim$1 dB. The main reason is the fact that the guard bandwidth is sufficient to achieve equal-quality DPN estimation under the same PNR.

VI. Conclusion

This paper employed the DA-PNS and the PA-PSN schemes to extend the transmission distance of a 100-GHz OFDM-RoF system, with deteriorated ICI and PE caused by the DPN. Because the DPN increases with greater dispersion and/or wider laser linewidth, the QPSK OFDM signal with 10.3-MHz linewidth was unable to reach the FEC limit after 150-km fiber. Employing the PNS schemes enabled the extension of the maximum fiber transmission distance to beyond 150 km with sensitivity penalties of $<\sim$2 dB, with a linewidth of 1.5 $\sim$ 10.3 MHz. In addition, the pilot tone in the PA-PNS scheme takes addtional power to reduce the signal power to an equivalent degree; therefore, the PA-PNS scheme underperforms the DA-PNS scheme in the most cases, and may even result in a sensitivity penalty, considering that the DPN is not critical. The DA-PNS scheme does not require additional overhead for optical power and electrical/optical components; however, it incurs higher computational complexity and the bandwidth of the estimated DPN must be truncated to avoid error propagation. Thus, the transmission penalty caused by the residual DPN might be higher in the DA-PNS scheme, while the PA-PNS scheme maintains the penalty variation to $<$1 dB, making the signal insensitive to transmission distance over distance of 0 $\sim$ 150 km.

References

[1] T. Kuri, K. Kitayama, and Y. Takahashi, "A single light-source configuration for full-duplex 60-GHz-band radio-on-fiber system," *IEEE Trans. Microw. Theory Techn.*, vol. 51, no. 2, pp. 431–439, Feb. 2003.

[2] J. Yu, Z. Jia, L. Yi, Y. Su, G.-K. Chang, and T. Wang, "Optical millimeter wave generation or up-conversion using external modulator," *IEEE Photon. Technol. Lett.*, vol. 18, no. 1, pp. 265–267, Jan. 2006.

[3] M.Weiß, M. Huchard, A. Stöhr, B. Charbonnier, S. Fedderwitz, and D. S. Jäger, "60-GHz photonic millimeter-wave link for short- to medium-range wireless transmission up to 12.5 Gb/s," *J. Lightw. Technol.*, vol. 26, no. 15, pp. 2424–2429, Aug. 1, 2008.

[4] Z. Jia, J. Yu, D. Qian, G. Ellinas, and G. K. Chang, "Experimental demonstration for delivering 1-Gb/s OFDM signals over 80-km SSMF in 40-GHz radio-over-fiber access systems," presented at the Opt. Fiber Commun., San Diego, CA, USA, 2008, Paper JWA 108.

[5] G. H. Nguyen, B. Cabon, and Y. Le Guennec, "Generation of 60-GHz MB-OFDM signal-over-fiber by up-conversion using cascaded external modulators," *J. Lightw. Technol.*, vol. 27, no. 11, pp. 1496–1502, Jun. 2009.

[6] A. Ng'oma, M. Sauer, F. Annunziata, W. J. Jiang, C. T. Lin, J. Chen, P. T. Shi, and S. Chi, "14 Gbps 60 GHz RoF link employing a simple system architecture and OFDM modulation," presented at the Int. Topical Meeting Microw. Photon., Valencia, Spain, Oct. 2009.

[7] C. T. Lin, J. Chen, P. T. Shih, W. J. Jiang, and S. Chi, "Ultra-high data-rate 60 GHz radio-over-fiber systems employing Optical frequency multiplication and OFDM formats," *J. Lightw. Technol.*, vol. 28, no. 16, pp. 2296–2306, Aug. 2010.

[8] J. B. Georges, "Thoughts on the future of small-cell backhaul," presented at the Conf. IEEE Communications Society, Santa Clara, CA, USA, Feb. 2013.

[9] J. Zhang, J. Yu, N. Chi, Z. Dong, X. Li, and G. K. Chang, "Multichannel 120-Gb/s data transmission over 2 $\times$ 2 MIMO fiber-wireless link at W-band," *IEEE Photon. Technol. Lett.*, vol. 25, no. 8, pp. 780–783, Mar. 2013.

[10] X. Pang, A. Caballero, A. Dogadaev, V. Arlunno, R. Borkowski, J. S. Pedersen, L. Deng, F. Karinou, F. Roubeau, D. Zibar, X. Yu, and I. T. Monroy, "100 Gbit/s hybrid optical fiber-wireless link in the W-band (75–110 GHz)," *Opt. Exp.*, vol. 19, pp. 24944–24949, Dec. 2011.

[11] J. Yu, X. Li, and N. Chi, "Faster than fiber: over 100-Gb/s signal delivery in fiber wireless integration system," *Opt. Exp.*, vol. 21, pp. 22885–22904, Sep. 2013.

[12] A. Kanno, K. Inagaki, I. Morohashi, T. Sakamoto, T. Kuri, I. Hosako, T. Kawanishi, Y. Yoshida, and K. Kitayama, "40 Gb/s W-band (75–110 GHz) 16-QAM radio-over-fiber signal generation and its wireless transmission," *Opt. Exp.*, vol. 19, pp. B56–B63, Jul. 2011.

[13] H. T. Huang, C. T. Lin, C. H. Ho, W. L. Liang, C. C. Wei, Y. H. Cheng, and S. Chi, "High spectral efficient W-band OFDM-RoF system with direct-detection by two cascaded single-drive MZMs," *Opt. Exp.*, vol. 21, pp. 16615–16620, Jul. 2013.

[14] W. R. Peng, "Analysis of laser phase noise effect in direct-detection optical OFDM transmission," *J. Lightw. Technol.*, vol. 28, no. 17, pp. 2526–2536, Aug. 2010.

[15] C. C. Wei and J. Chen, "Study on dispersion-induced phase noise in an optical OFDM radio-over-fiber system at 60-GHz band," *Opt. Exp.*, vol. 18, pp. 20774–20785, Sep. 2010.

[16] W. Chung, "A matched filtering approach for phase noise suppression in CO-OFDM systems," *IEEE Photon. Technol. Lett.*, vol. 22, no. 24, pp. 1802–1804, Dec. 2010.

[17] S. Wu, P. Liu, and Y. Br-Ness, "Phase noise estimation and mitigation for OFDM Systems," *IEEE Trans. Wireless Commun.*, vol. 5, no. 12, pp. 3616–3625, Dec. 2006.
[18] C. Yang, F. Yang, and Z. Wang, "Orthogonal basis expansion-based phase noise estimation and suppression for CO-OFDM systems," *IEEE Photon. Technol. Lett.*, vol. 22, no. 1, pp. 51–53, Dec. 2010.
[19] C. T. Lin, C. C. Wei, and M. I. Chao, "Phase noise suppression of optical OFDM signals in 60-GHz RoF transmission system," *Opt. Exp.*, vol. 19, pp. 10423–10428, May 2011.
[20] C. C. Wei, C. T. Lin, M. I. Chao, and W. J. Jiang, "Adaptively modulated OFDM RoF signals at 60 GHz over long-reach 100-km transmission systems employing phase noise suppression," *IEEE Photon. Technol. Lett.*, vol. 24, no. 1, pp. 49–51, Jan. 2012.
[21] S. Randel, S. Adhikari, and S. L. Jansen, "Analysis of RF-pilot-based phase noise compensation for coherent optical OFDM systems," *IEEE Photon. Technol. Lett.*, vol. 22, no. 12, pp. 1288–1290, Aug. 2010.
[22] S. L. Jansen, I. Morita, N. Takeda, and H. Tanaka, "20-Gb/s OFDM transmission over 4,160-km SSMF Enabled by RF-pilot tone phase noise compensation," presented at the Optical Fiber Commun. Conf., Anaheim, CA, USA, 2007, Paper PDP 15.
[23] W. R. Peng, I. Morita, and H. Tanaka, "Digital phase noise estimation and mitigation approach for direct-detection optical OFDM transmissions," presented at the Eur. Conf. Opt. Commun., Torino, Italy, 2010, Paper Tu.3.C.3.
[24] H. T. Huang, W. L. Liang, C. T. Lin, C.-C. Wei, and S. Chi, "100-GHz DD-OFDM-RoF system over 150-km fiber transmission employing pilot-aided phase noise suppression and bit-loading algorithm," *Opt. Exp.*, vol. 22, pp. 3938–3943, Feb. 2014.
[25] L. Tomba, "On the effect of wiener phase noise in OFDM systems," *IEEE Trans. Commun.*, vol. 46, no. 5, pp. 580–583, May 1998.
[26] M. S. El-Tanany, Y. Wu, and L. Hazy, "Analytical modeling and simulation of phase noise interference in OFDM-based digital television terrestrial broadcasting systems," *IEEE Trans. Broadcast.*, vol. 47, no. 1, pp. 20–31, Mar. 2001.
[27] T. Okoshi, K. Kikuchi, and A. Nakayama, "Novel method for high resolution measurement of laser output spectrum," *Electron. Lett.*, vol. 16, pp. 630–631, Jul. 1980.

Chia-Chien Wei received the Ph.D. degrees in electro-optical engineering from National Chiao Tung University, Hsinchu City, Taiwan, and electrical engineering from the University of Maryland, Baltimore, MD, USA, in 2008.

In 2011, he joined National Sun Yat-sen University, Kaohsiung, Taiwan, where he is currently an Assistant Professor in the Department of Photonics. His current research interests include optical and electrical signal processing, advanced modulation formats, optical access networks, and radio-over-fiber systems.

Chun-Ting Lin received the B.S. and M.S. degrees in material science and engineering from National Tsing Huang University, Hsinchu, Taiwan, in 1997 and 2001, respectively, and the Ph.D. degree in electro-optical engineering from National Chiao Tung University, Hsinchu, in 2007.

From 2007 to 2009, he was a Research Associate with the Department of Photonics, National Chiao Tung University. In 2009, he joined the Faculty of National Chiao Tung University, where he is currently an Associate Professor with the Institute of Photonic System. His research interests are radio-over-fiber systems, optical millimeter/sub-terahertz wave generation and application, optical data formats, and opto-electronic packages.

Hou-Tzu Huang received the B.S. degree from the Department of Photonics from National Chiao Tung University, Hsinchu, Taiwan, in 2012, where he is currently working toward the Ph.D. degree with the Institute of Photonics System. His current research interests include radio-over-fiber systems, fiber/wireless MIMO technique, and digital signal processing.

Wan-Ling Liang received the B.S. degree from the Department of Physics, National Changhua University of Education, Changhua, Taiwan, in 2011, and the M.S. degree in the Institute of Lighting and Energy Photonics, National Chiao Tung University, Hsinchu, Taiwan, in 2013.

Sien Chi received the B.S.E.E. degree from National Taiwan University, Taipei, Taiwan, and the M.S.E.E. degree from National Chiao Tung University, Hsinchu, Taiwan, in 1959 and 1961, respectively. He received the Ph.D. degree in electrophysics from Polytechnic Institute, Brooklyn, NY, USA, in 1971.

From 1971 to 2004, he was a Professor at National Chiao Tung University. From 1998 to 2001, he was the Vice President of the National Chiao Tung University. He is currently a Chair Professor at National Chiao Tung University. His research interests are optical-fiber communications, fast and slow light, passive optical networks, and microwave photonics. He is a Fellow of the Optical Society of America.